Environmental Pollution 273 (2021) 116490

Contents lists available at ScienceDirect

Environmental Pollution

journal homepage: www.elsevier.com/locate/envpol

Automatic detection and quantification of floating marine macro-litter in aerial images: Introducing a novel deep learning approach connected to a web application in R☆

Odei Garcia-Garin [a, *], Toni Monleón-Getino [b, c, d], Pere López-Brosa [b, c], Asunción Borrell [a], Alex Aguilar [a], Ricardo Borja-Robalino [b, c], Luis Cardona [a], Morgana Vighi [a]

[a] Institute of Biodiversity Research (IRBio) and Department of Evolutionary Biology, Ecology and Environmental Sciences, Universitat de Barcelona, Barcelona, Spain
[b] Department of Genetics, Microbiology and Statistics, Universitat de Barcelona, Barcelona, Spain
[c] BIOST[3], Spain
[d] GRBIO (Research Group in Biostatistics and Bioinformatics), Barcelona, Spain

ARTICLE INFO

Article history:
Received 24 June 2020
Received in revised form
7 January 2021
Accepted 8 January 2021
Available online 11 January 2021

Keywords:
Remote sensing
Machine learning
Unmanned aerial vehicles
Convolutional neural network
Marine litter

ABSTRACT

The threats posed by floating marine macro-litter (FMML) of anthropogenic origin to the marine fauna, and marine ecosystems in general, are universally recognized. Dedicated monitoring programmes and mitigation measures are in place to address this issue worldwide, with the increasing support of new technologies and the automation of analytical processes. In the current study, we developed algorithms capable of detecting and quantifying FMML in aerial images, and a web-oriented application that allows users to identify FMML within images of the sea surface. The proposed algorithm is based on a deep learning approach that uses convolutional neural networks (CNNs) capable of learning from unstructured or unlabelled data. The CNN-based deep learning model was trained and tested using 3723 aerial images (50% containing FMML, 50% without FMML) taken by drones and aircraft over the waters of the NW Mediterranean Sea. The accuracies of image classification (performed using all the images for training and testing the model) and cross-validation (performed using 90% of images for training and 10% for testing) were 0.85 and 0.81, respectively. The Shiny package of R was then used to develop a user-friendly application to identify and quantify FMML within the aerial images. The implementation of this, and similar algorithms, allows streamlining substantially the detection and quantification of FMML, providing support to the monitoring and assessment of this environmental threat. However, the automated monitoring of FMML in the open sea still represents a technological challenge, and further research is needed to improve the accuracy of current algorithms.

1. Introduction

Marine litter, defined as *any persistent, manufactured or processed solid material discarded, disposed of, abandoned, or lost in the marine and coastal environment* (UNEP, 2005), is ubiquitous in all marine compartments worldwide (*e.g.*, Arcangeli et al., 2018; Cózar et al., 2014; Suaria et al., 2020). It poses a potential threat to the marine fauna, including invertebrates (*e.g.*, Digka et al., 2018), fish (*e.g.*, Garcia-Garin et al., 2019; 2020d), marine mammals (*e.g.*, De Stephanis et al., 2013), and turtles (*e.g.*, Schuyler et al., 2014). Floating marine macro-litter (FMML, *i.e.*, objects > 2.5 cm; Galgani et al., 2013; GESAMP, 2019) of anthropogenic origin is particularly harmful, because of its potential to entangle all sort of marine organisms (*e.g.,* fishes, turtles, marine mammals; Deudero & Alomar, 2015), and of being ingested by marine fauna, especially large filter-feeding species (Garcia-Garin et al., 2020c). Monitoring its density and distribution patterns through standardized methodologies (Van Sebille et al., 2020) is highly needed to assess the extent of this environmental threat (GESAMP, 2015; UNEP 2016).

FMML presence and distribution have been traditionally assessed through manta trawl nets (*e.g.*, Lebreton et al., 2018), indicator species (*e.g.*, Domènech et al., 2019), and observer-based

☆ This paper has been recommended for acceptance by Eddy Y. Zeng.

* Corresponding author.
E-mail address: odei.garcia@ub.edu (O. Garcia-Garin).

https://doi.org/10.1016/j.envpol.2021.116490

methods applied from vessels (Arcangeli et al., 2018; Suaria and Aliani, 2014) or manned aircraft (*e.g.*, Garcia-Garin et al., 2020a; Pichel et al., 2012), which are often time-demanding and expensive techniques. Although traditional observer-based methods present many advantages (*e.g.*, precise identification of targets, absence of constraints related to the duration of the camera battery charge or the storage space), alternative remote sensing methods offer distinct advantages, such as more objective and reproducible results, and the possibility to re-analyse the recorded images for other investigations (Garcia-Garin et al., 2020b; Veenstra and Churnside, 2012). Thus, either passive (*e.g.*, RGB video, digital camera, multispectral, hyperspectral) or active (*e.g.*, lidar, radar) sensors coupled to aerial vehicles (*e.g.*, aircraft, drones, satellites) can be excellent tools to quantify and monitor the distribution of FMML (Garcia-Garin et al., 2020b; Kikaki et al., 2020; Martínez-Vicente et al., 2019; Maximenko et al., 2019; Veenstra and Churnside, 2012; Topouzelis et al., 2019). Nevertheless, these techniques can also be highly time-consuming if the analysis of the images is done manually by one or more trained scientists, (*e.g.*, Garcia-Garin et al., 2020a). The development of algorithms to automatically detect FMML in aerial images, and thus streamline the analytical process, is critical for the successful implementation of these techniques.

In the last decade, machine learning models have shown good results in the analysis of environmental processes (Quetglas et al., 2011). In particular, deep learning models using Convolutional Neural Networks (CNNs) have been widely applied due to their ability to recognize features and patterns contained in large datasets of images or videos (Guirado et al., 2019; Velandia et al., 2017). So far, few algorithms have been developed to detect and identify FMML in digital images (Kylili et al., 2019). To the best of our knowledge, none of them were trained or tested to recognize floating litter items using aerial RGB images. Some authors (*e.g.*, Garaba and Dierssen 2018; Garaba et al., 2018; Goddijn-Murphy and Dufaur, 2018; Goddijn-Murphy et al., 2018; Kikaki et al., 2020; Topouzelis et al., 2019) used spectral information to develop models that could automatically detect litter items and could be applied to aerial imagery, and others (*e.g.*, Kylili et al., 2019) successfully applied CNN models to automatically detect FMML in images taken few meters above the water surface. Remote sensing of FMML is in its infancy (Garaba et al., 2018; Maximenko et al., 2019), and despite recent improvements and encouraging results, algorithms able to automatically detect FMML in aerial RGB images are still lacking.

The aim of the present study was to develop an R (R Core Team, 2020) library based on a deep learning approach, to automatically detect and quantify FMML in aerial images of the sea surface taken from drones and aircraft. After validating the accuracy of the package, we also propose the implementation of such approach through a web-oriented application based on the Shiny package. The development of user-friendly applications for monitoring the presence of floating marine litter would facilitate the implementation of routine monitoring programmes of this threat, in compliance with current regional and national environmental regulations.

2. Materials and methods

2.1. Survey area

Aerial images were obtained during photographic surveys performed by drones and manned aircraft between 2017 and 2019 over the marine area located between *Delta de l'Ebre* and *Cap de Creus* (NW Mediterranean, Fig. 1). Surveys with drones were performed on May 16th and June 3rd 2017 at Blanes, June 6th 2018 at *Cap de Creus* and February 4th 2019 *at Delta de l'Ebre*. Surveys with aircraft were performed on January 24th and March 14th 2018 at *Delta de l'Ebre*. To minimize the effect of wind and sun glint on the detection

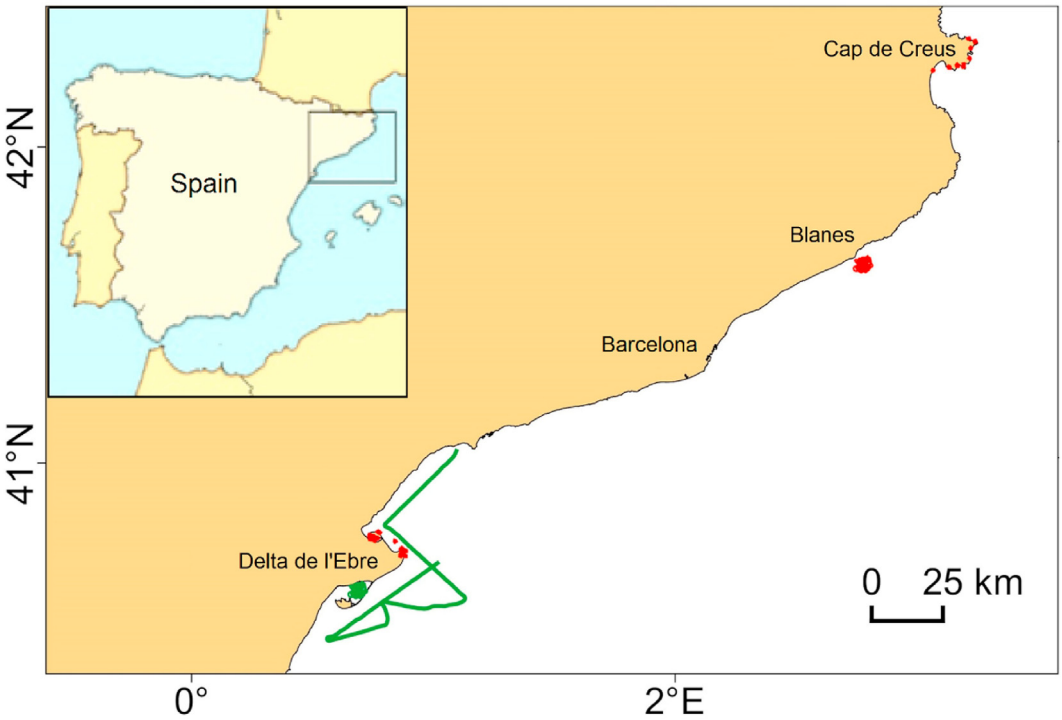

Fig. 1. Map of the study area indicating the GPS tracks and locations of the drone (red) and aircraft (green) surveys performed over the areas of *Cap de Creus*, Blanes and *Delta de l'Ebre*. (For interpretation of the references to color in this figure legend, the reader is referred to the Web version of this article.)

of FMML, all surveys were conducted with low wind force (*i.e.*, Beaufort sea state < 3) and avoiding the hours of the day when the sun was higher on the horizon.

2.2. Photographic surveys

2.2.1. Drone surveys

Four different types of drones were used: (1) a fixed-wing HP1 equipped with an RGB camera Sony ILCE-6000 (6000 × 4000 pixels), and (2) a multi-rotor *Topografia* equipped with an RGB camera Sony Alpha 7 R (7952 × 5304 pixels) off Blanes, (3) a Phantom 3 Advanced equipped with an RGB camera FC300S (4000 × 3000 pixels) at *Cap de Creus*, and (4) a DJI Mavic Pro equipped with an RGB camera FC220 (4000 × 3000 pixels) at *Delta de l'Ebre*. All images were taken with the cameras placed in the nadir position at altitudes ranging from 20 to 120 m, and with a ground sampling distance ranging between 0.6 and 3.6 cm pixel^{-1}. A total of 3900 images were recorded, of which the 121 taken by (1) and 200 by (2), were shot over positive controls (*i.e.*, a series of FMML of known size and type) deployed from a boat (Fig. 2). The remaining 2589 images taken by (3) and 990 by (4) were recorded over natural sea conditions.

2.2.2. Aircraft surveys

Aircraft surveys were performed with a high-wing aircraft (Partenavia P- 68) flying at a constant groundspeed of 90 knots (166 km h^{-1}) and an altitude ranging from 230 to 300 m, equipped with a Canon EOS REBEL SL1 (5184 × 3456 pixels) camera connected to the aircraft GPS signal. The camera, placed under the aircraft and pointed at 90° to the ground, was controlled from a tablet through the Waldo Flight Control System software. Ground sampling distance ranged between 2.5 and 3.3 cm pixel^{-1}. A total of 3000 images were taken, 25 of which were obtained over the same positive controls used for the drone surveys (Fig. 3A).

2.3. Image pre-processing

Images were inspected by a trained scientist to detect the presence of FMML, and a subset of 796 images was labelled according to the following categories: (1) containing FMML (398 images), and (2) not containing FMML (398 images). The trained scientist had a proven experience in detecting floating litter in aerial imagery as he had previously reviewed thousands of images for the purpose and he was also involved in the field observations. However, all doubtful items were checked by a second experienced researcher. As thousands of images per category are usually needed to train properly a deep learning model (Sun et al., 2017), the available images for each category were not enough. Thus, the number of images was increased through data augmentation (*i.e.*, shifting, zooming, rotation, etc. of the available images) as in Kylili et al. (2019), to obtain a larger dataset of 1860 images containing FMML and 1863 images without FMML. Examples of aerial images taken by drones and aircraft over positive controls, FMML and sea water, are shown in Fig. 3.

2.4. Deep learning algorithm

Consistently with Kylili et al. (2019), an algorithm to automatically detect FMML in aerial images was developed by applying a deep learning approach based on a CNN architecture. While other

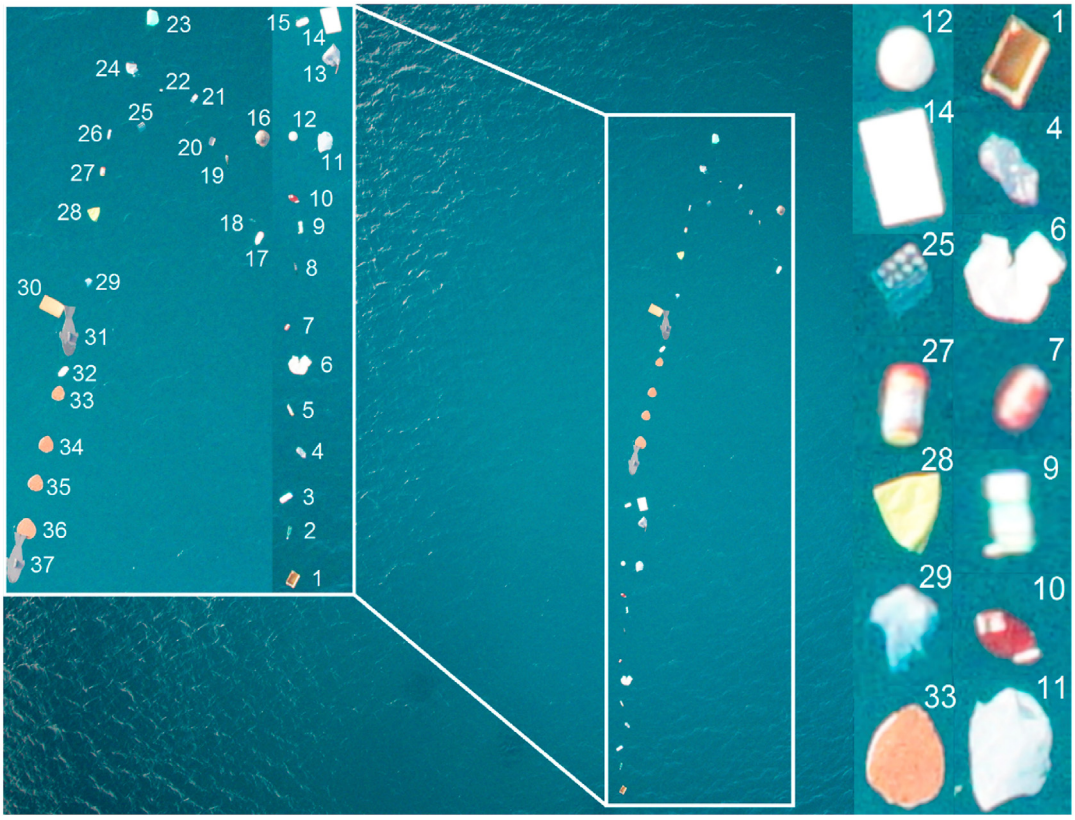

Fig. 2. Example of an aerial image taken by the drone over a series of known items with neutral or positive buoyancy attached to a line deployed from a boat (*i.e.*, our positive control). 1 = crate; 2–4, 8, 19 = bottles; 5, 7, 22, 26 = cans; 6 = sack; 9, 21 = tetra-brik packages; 10 = net; 11,13, 23, 24 = bags; 12 = ball; 14, 30 = boards; 15, 17, 32 = drum; 16 = turtle carapax; 18 = six pack rings; 20, 25 = trays; 27 = jar; 28 = balloon; 29 = towels; 31, 33–37 = polystyrene.

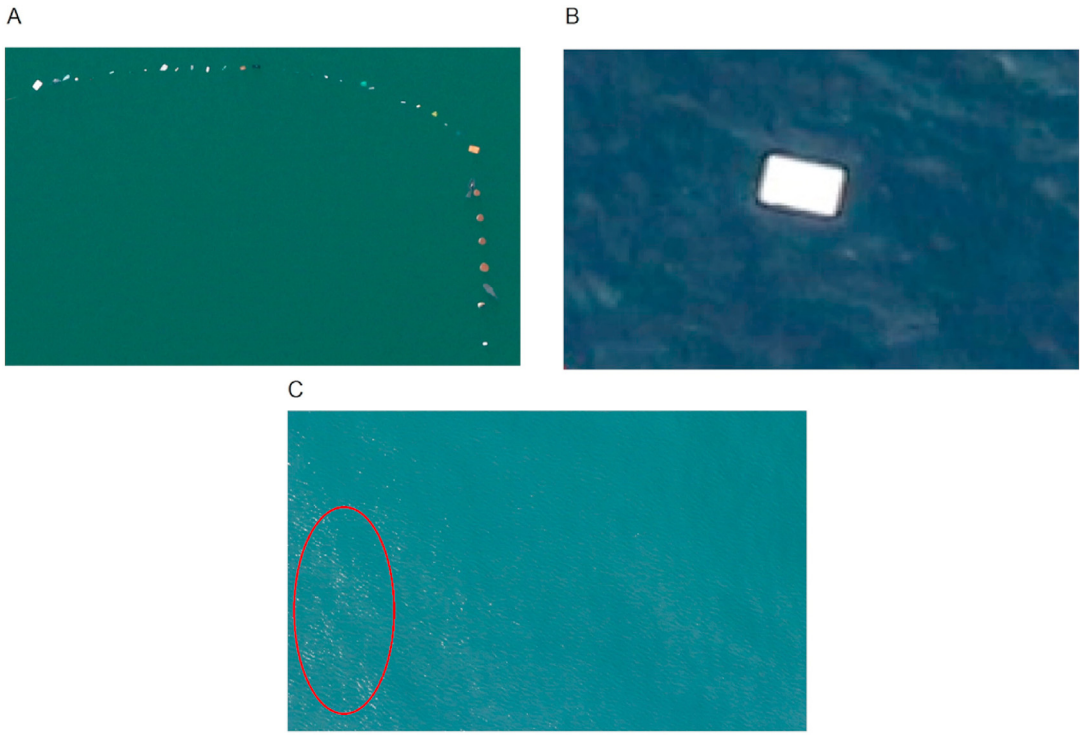

Fig. 3. Examples of aerial images ((A) positive controls as in Fig. 2, (B) board and (C) sea water with an area affected by sun glint circled in red) taken from aircraft and drones. Images were cropped to improve the visibility of items. (For interpretation of the references to color in this figure legend, the reader is referred to the Web version of this article.)

machine learning methods need a set of features to feed the classifier, deep learning based on CNNs trains and recognizes the spatial patterns of the targets using a series of features that are inside its native structure (Gonçalves et al., 2020b; Guirado et al., 2019).

A total of 34 different models (Table S2) were developed in R (R Core Team, 2020) with the following CNN architectures:

Architecture 1: 1 Convolutional layer (Hyperparameters) + 1 Pooling layer (size = 1 × 1) + 1 Convolutional layer (Hyperparameters) + 1 Pooling layer (size = 1 × 1) + 1 Fully connected (500 neurons, Tanh) + 1 Fully connected (20 neurons) + Softmax.

Architecture 2: 2 Convolutional layers (Hyperparameters) + 1 Pooling layer (size = 2 × 2) + 2 Convolutional layers (Hyperparameters) + 1 Pooling layer (size = 2 × 2) + 1 Fully connected (3200 neurons, ReLU) + 1 Fully connected (1000 neurons) + Softmax.

After testing the different models (Table S2), the second CNN architecture, showed in Fig. 4, was selected as the best option. The optimization of the value of the hyperparameters was decisive to obtain the maximum accuracy in the training and testing sets without falling into overfitting. The optimal parameters were: Kernel = 3 × 3, learning rate = 0.0001, batch size = 100, momentum = 0.9, optimizer = Adam, epochs = 400.

Such architecture was built through the use of three types of layers: (1) the convolutional layer, which extracts features from the input images at different levels of hierarchy, (2) the pooling layer, which is a reduction operation used to increase the abstraction level of the extracted features, and (3) fully connected and hidden layers, which are used as classifiers at the end of the pipeline (Fig. 4). Convolutional layers were composed of the convolution of small groups of pixels (3 × 3) extracted from the input image by a kernel matrix with the addition of a bias; these parameters were previously established during the network learning process. The ReLU activation function, which complies with the basic property of introducing non-linearity in the system (Shridhar et al., 2019; Velandia et al., 2017), was applied to facilitate the optimization process for binary classifications. A pooling layer was also applied to each convolutional layer to perform a subsampling process with the most relevant features. A process of vectorization and concatenation of data (flattened) was carried out, allowing the application of two completely connected layers that made the convolutional layers determine the learning process of the most relevant characteristics.

The softmax regression, which is often used in neural networks to map the non-normalized output to a probability distribution of a defined number of predicted outputs, was used to obtain the prediction of 2 categories (*i.e.*, FMML, no FMML). The softmax function (Bishop, 2006) took as input a vector of K real numbers from the hidden layers and normalized them into a probability distribution consisting of K probabilities proportional to the exponentials of the input numbers. The learning of the neural network was done through the backpropagation process. Thus, the parameters were estimated and updated until the network reached the optimal solution through the estimation of the weight matrix and the vector of biases within the hyperconus of feasible solutions (Fig. 5) that allowed the convergence of the model with the best performance (Shridhar et al., 2019; Velandia et al., 2017).

A library named AIImagePred (automatic image recognition and prediction based on deep learning) was developed in R (R Core Team, 2020) to classify images in 2 classes, based on the CNN model. AIImagePred was developed based on other well-known libraries in the deep-learning environment, such as Keras (Falbel et al., 2018) and Mxnet (Chen et al., 2018), as a general-purpose package for image recognition and prediction based on CNNs. As AIImagePred includes an algorithm that splits the image into multiple parts, individual or multiple images can be processed, without prior separation or segmentation.

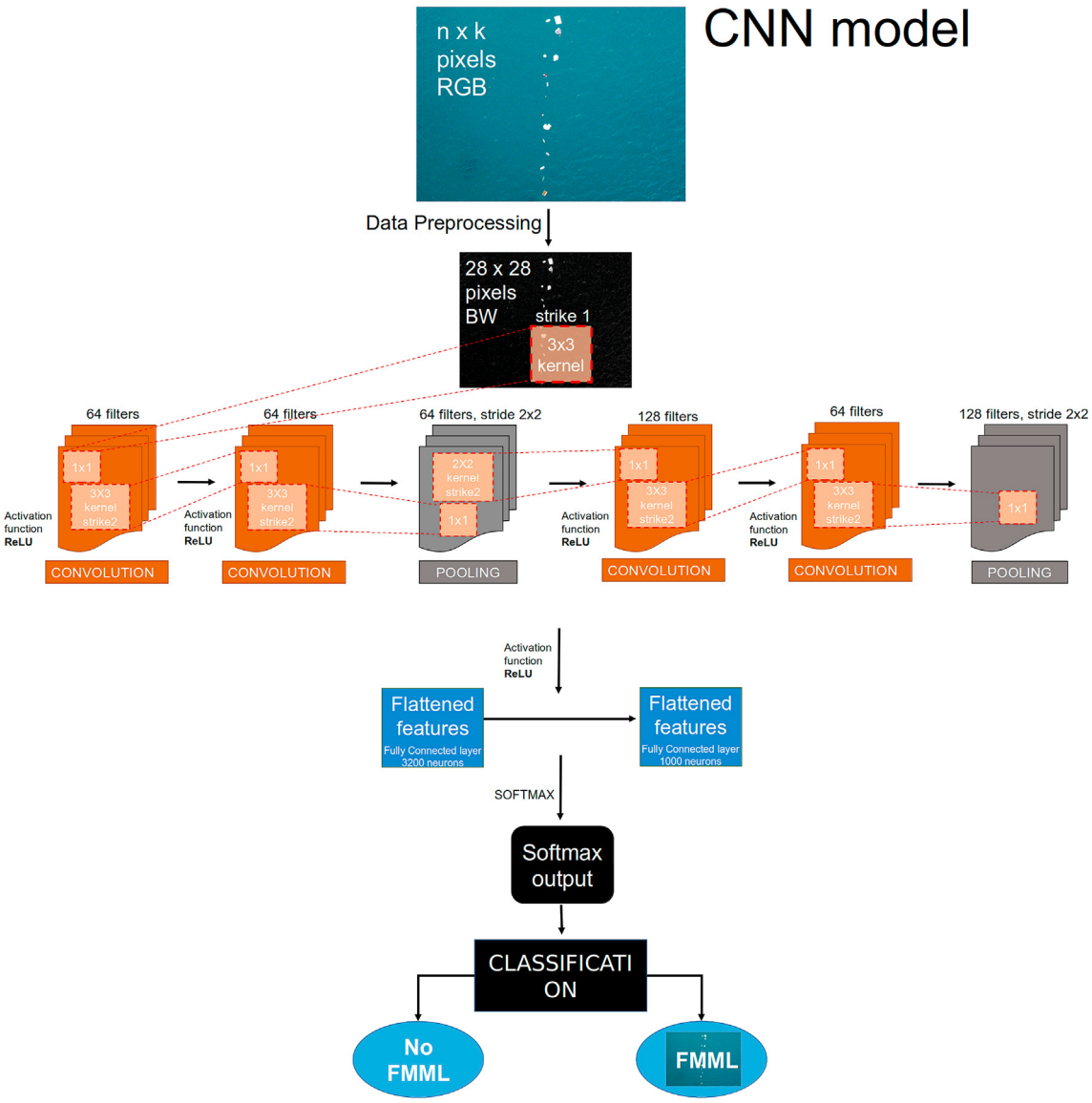

Fig. 4. Convolutional neural network workflow. The processed image was a positive control image of marine litter captured from a drone.

The two main functions of AIImagePred (Table 1) were: (1) image. trainimages.DL.algorithm_multiclass(), which creates and trains the CNN model for the classification of aerial images based on the architecture in Fig. 4; and (2) split. predict.count.multiclass(), which uses the pre-trained CNN model to classify a testing set of images in a series of 2 predefined classes. Thus, once the image is split in multiple cells (we recommend splitting images into at least 25 cells), the algorithm classifies each cell of the image as containing FMML or not.

To guarantee the functionality of the algorithm, aerial images must be taken in nadir position with a ground sampling distance of at least 3.6 cm pixel^{-1}. To further improve the algorithm accuracy, aerial images should be taken with sea state conditions of Beaufort < 3 and avoiding the times of the day when the sun is higher on the horizon to minimize the effect of the wind and the sun glint on the detection of FMML.

The convolutional layering and pooling operations are represented by Equation (1). The resulting matrices of the convolutional layers (C) were flattened. Equation (2) represents the complete model including the densely connected layers (Dumoulin and Visin, 2018; Kuo, 2016):

$$C = P\left[a\left(\sum_{q=1}^{128} a\left(\sum_{q=1}^{128}\left(P\left[a\left(\sum_{q=1}^{64} a\left(\sum_{q=1}^{64} I{*}K_{1,q}^{1} + b_q^1\right){*}K_{1,q}^{2} + b_q^2\right)\right]_{\max(2i,2j)}\right){*}K_{1,q}^{3} + b_q^3\right){*}K_{1,q}^{4} + b_q^4\right)\right]_{\max(2i,2j)} \quad (1)$$

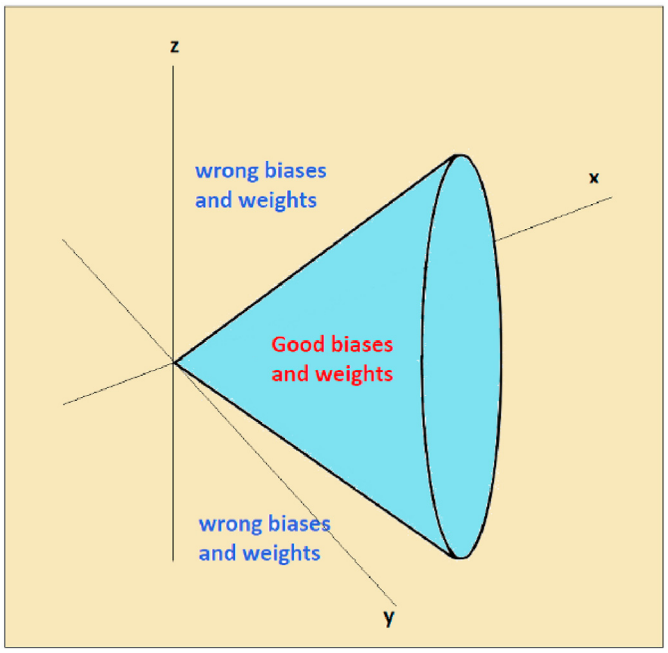

Fig. 5. Three-dimensional region of feasible solutions for weights and biases in the case of binary classification. The axes represent the dimensions in the convolutional space (x = length, y = width, z = depth). Each point within the cone represents the optimal value for each convolutional layer to extract the characteristics of the image in the best way.

$$\widehat{y} = softmax\Big[\sum_{q=1}^{1000}\Big[a\Big(\sum_{q=1}^{3200} C_a \cdot K_{1,q}^{5} + b_q^5\Big)\Big] \cdot k_{1,q}^{6} + b_q^6\Big] \quad (2)$$

where:

- $K_{p,q}^{l}$ = Kernel matrix; l = number of the layer; p = origin; q = filter number.
- b_q^l = biases.
- $P_{max(2i,2j)}$ = pooling layer (max-pooling).
- a = activation function "ReLU".
- $\widehat{y}$ = output (FMML − not FMML).
- $(*)$ = convolution; $(\cdot)$ = matrix product.
- C = convolution and pooling layer process.
- C_a = vectorization and concatenation of the output C.

2.5. Accuracy assessment

A total of 3723 images (1860 with FMML, 1863 without FMML) were used to train/test the model during classification, 90% and 10% of which were used to train and test the model, respectively, during cross-validation. The overall accuracy of the model results was assessed during both processes through four parameters: accuracy, precision, recall, and F1-score. Accuracy (Equation (3)) represents the fraction of all the images processed that were correctly classified as containing FMML or not containing FMML, precision (Equation (4)) represents the fraction of images classified as containing FMML that actually belonged to that class, while recall (Equation (5)) represents the fraction of correctly labelled images within each class. Accuracy, precision, and recall values vary between 0 and 1. F1-score (Equation (6)) represents a balance between precision and recall (Fawcett, 2006) and its value increases with the performance of the model (Bekkar et al., 2013). The accuracy assessment was obtained from the training and testing sets over 400 epochs.

$$Accuracy = \frac{TP + TN}{N} \quad (3)$$

$$Precision = \frac{TP}{TP + FP} \quad (4)$$

$$Recall = \frac{TP}{TP + FN} \quad (5)$$

$$F1 = \frac{2{*}TP}{2{*}TP + FP + FN} \quad (6)$$

where:

- TP = True positive: images with FMML well classified
- TN = True negative: images without FMML well classified.
- FP = False positive: images without FMML misclassified.
- FN = False negative: images with FMML misclassified.
- N = Total images analysed.

The repeatability of the method was tested by processing 10 runs of randomly selected image sets (n = 3723, 90% of which were used for training, and 10% for testing).

2.6. Application based on the Shiny package

An interactive web application was built in R, based on a simpler version of the CNN model developed (see supplementary material:

Table 1
Functions contained in the library AIImagePred.

Function	Features	Arguments
image.trainimages.DL.algorithm_ multiclass()	Algorithm that extracts features from the image to train a CNN-based deep learning model using the architecture presented in Fig. 4. The algorithm creates, tests, and optimizes the model to be used for image classification.	Function1(dir.imag.training, dictionary = c(plastic = 0, sin = 1), size_foto = 28, check.accuracy = T, Do.saveRDS = T, Do.save.model = T, percent.CV = 0.9, num.round = 400)
split.predict.count.multiclass()	Algorithm that automatically identifies FMML in aerial images: it reads the trained images, and predicts their class. The algorithm allows the analysis of the whole image or its division in equal parts, after converting it to multiple images.	Function2(train.images.dir, name.files.images, predict.test.images.dir, size_foto = 28, dictionary = c(plastic = 0, sin = 1), use.model = T, nom.model.saved = "prova_model.RData", num.round = 400, n.div = 5, my.opinion = NULL).

Table S2, test 2 & Fig. S1), using the Shiny package (Chang et al., 2020). The scope of the application was to create a user-friendly interface that could allow the detection of FMML in any aerial image that is uploaded by the user.

2.7. Hardware requirements

Image processing and numerical calculations under pre-built or designed CNN architectures require high-level processors with special features in their RAM and graphic cards (NVIDIA). Currently, the most popular mean of developing Artificial Intelligence is the computer running NVIDIA, closely followed by Raspberry Pi. Due to the high computational cost required to train the network using cross-validation and the high quality of the images analysed, the pre- and post-processing of the network were developed using a HPC Computer Server, 40 cores Xeon SP 4114 2,2 GHz, within the premises of the University of Barcelona (Spain).

Despite the new Raspberry Pi 4 - Model B of 8 gigabytes could allow the classification of images (testing phase), this option was discarded due to its too expensive training in the metric “execution time".

3. Results

3.1. CNN model accuracy

The function image.trainimages.DL.algorithm_multiclass() was used to compute the CNN model, following the CNN architecture presented in Fig. 4. The accuracy of the CNN model was tested during classification and cross-validation. In a first step, all the labelled images were used to test the total accuracy (n = 3723, 1860 images with FMML, 1863 images without FMML). The classification accuracy was 0.85 (TP = 94%, TN = 76%) using all images as both training and testing set, and 0.81 (TP = 84%, TN = 78%) after cross-validation (n = 3723, 90% images used for training, 10% for testing) (Table 2). The maximum accuracies attained by cross-validation during training and testing were 0.90 and 0.85, respectively. Images mis-classified were those that were most affected by sun glint (Fig. 3B). It should be noted that the accuracy obtained during cross-validation was lower than that of classification because the first process uses different images for training and testing, while the same images are used for training and testing during classification.

The repeatability of the method was tested by processing 10 runs of randomly selected image sets (n = 3723, 90% images used for training, 10% for testing) using the AIImagePred function and computing the accuracy for each set. The mean classification accuracy was 0.85 ± 0.03 for the training sets and 0.79 ± 0.03 for the testing sets (Fig. 6).

3.2. Application based on Shiny language

A visual application, namely MARLIT, to detect and quantify FMML in aerial images, oriented to web applications, was developed through the Shiny package within the R programming language. The web application, accessible from a computer device, allowed: (1) uploading aerial images; (2) splitting images into multiple cells, (3) analysing them through the AIImagePred R library; (4) detecting FMML presence in each of the cells; and (5) quantifying its density in relation to the surface covered by the images, which is calculated from the metadata provided in the uploading phase, namely the height and focal distance. They are online for public test and use, and any possible improvements or suggestions from other researchers are warmly welcomed. The CNN model analyses each cell separately to determine if it contains FMML or not. By increasing the number of cells, the accuracy of the FMML density calculated by the application is improved, but the time needed for processing increases. The MARLIT application and the AIImagePred library can be downloaded from https://github.com/amonleong/MARLIT.

Fig. 7 shows an example of the application interface, where an image containing FMML is analysed, cells containing FMML are identified and FMML relative density is quantified.

4. Discussion

In this study, we applied CNN-based deep learning models to detect and quantify FMML in aerial images, we proposed their coupling to the AIImagePred library in R and their implementation on a web-oriented application based on the Shiny package. Results obtained from the application of the optimal CNN model to analyse 3723 aerial images recorded during drone and aircraft surveys showed good accuracies of FMML detection.

Our results further support the use of airborne sensors for inspecting the sea surface and detecting FMML. Studies based on these techniques for FMML monitoring have substantially increased within the last decade. Aerial photography is already being used for this aim at large scale, including for the monitoring of the “Great Pacific Garbage Patch” (Garaba et al., 2018; Lebreton et al., 2018) and of coastal areas of the Western Mediterranean Sea (Garcia-Garin et al., 2020a). However, when photographic methods are used, densities of FMML are not calculated through a common, standardized, and efficient algorithm, since image analyses are still often performed manually. Aerial photography methods should be coupled with efficient automated FMML detection processes to prove their effectiveness and to provide a valid alternative to replace traditional monitoring techniques.

The remote sensing of marine litter is a technological challenge and is currently in constant development (Martínez-Vicente et al.,

Table 2
Accuracy, precision, recall and F1-score of the CNN model here proposed to detect FMML in aerial RGB images and of those currently available for marine litter detection. * Mean values are shown.

	Method	Process	Accuracy	Precision	Recall	F1-score
This study	CNN	Classification	0.85	0.79	0.94	0.86
	CNN	Cross-validation (training)	0.85	0.81	0.91	0.86
	CNN	Cross-validation (testing)	0.81	0.82	0.84	0.83
Martin et al. (2018)	Random forest		–	0.08	0.40	0.13
Fallati et al. (2019)	CNN	Training	0.95	–	–	–
	CNN	Testing	-	0.54	0.44	0.49
Kylili et al. (2019)	CNN	Training	1	–	–	–
	CNN	Testing	0.99	-	-	-
Jakovljevic et al. (2020)*	CNN		–	0.82	0.59	0.66
Gonçalves et al. (2020a)	Random forest		–	0.73	0.74	0.75
Gonçalves et al. (2020b)	CNN		–	0.55	0.65	0.60

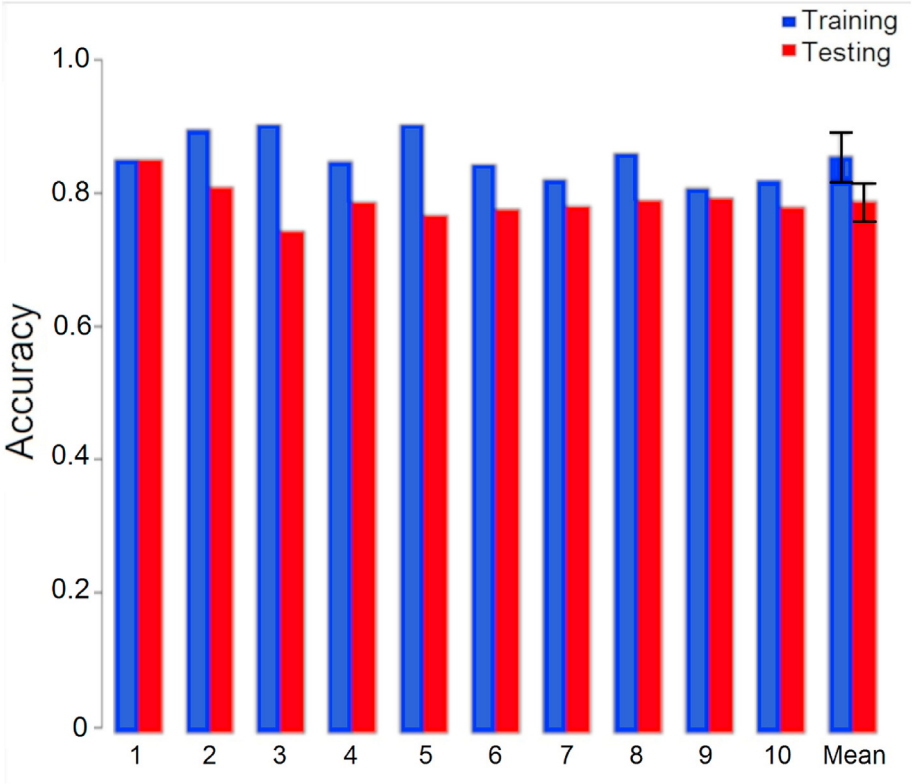

Fig. 6. CNN model accuracy assessed during 10 repeated cross-validation runs processing randomly selected image sets (n = 3723, 90% used for training, 10% for testing). Left columns represent the accuracy obtained for the training sets and right columns represent the accuracy obtained for the testing sets. The last two columns indicate the mean accuracy ± the standard deviation obtained within the 10 cross-validation runs.

2019; Maximenko et al., 2019). Remote sensing algorithms for beach monitoring are more advanced than those available for the sea surface, mainly because georeferenced orthomosaics are more easily produced from the overlapped photographs of beaches, where many reference points can be used for calibration (*e.g.*, trees, shrubs, plant logs). Furthermore, beach monitoring is less affected by environmental conditions such as perturbations on the sea surface caused by wind or sun glint, and the risk of losing unmanned vehicles is lower when flying over the land than over the sea surface (Fallati et al., 2019; Gonçalves et al., 2020b; Martin et al., 2018; Merlino et al., 2020). Conversely, monitoring FMML through remote sensing is further challenged by bright elements on the marine surface (*e.g.*, white caps, foam, waves, sun glint), cloud shadows (Dierssen and Garaba, 2020; Garaba and Dierssen, 2018; Matthews et al., 2017; Maximenko et al., 2019) and the fact that floating items can often be partially submerged in the water column (Van Sebille et al., 2020).

Machine learning algorithms have been used to automate marine litter recognition in aerial imagery, using, for instance, random forest (Gonçalves et al., 2020a, 2020b; Martin et al., 2018) or deep learning approaches (Fallati et al., 2019; Gonçalves et al., 2020b; Kako et al., 2020; Kylili et al., 2019). The main advantage of deep learning algorithms compared to their predecessors (*e.g.*, SVM, random forest, Multiple Regression) is that they can automatically identify the important features of an image without any human supervision, which makes them less time-demanding.

CNNs are the most popular deep learning architectures, inspired by the biological resemblance between the connectivity pattern of neurons and the organization of the animal visual cortex (Shridhar et al., 2019). Their effectiveness to identify images with hidden complex patterns (*e.g.*, Gonçalves et al., 2020b; Kylili et al., 2019) brought a raising interest on CNNs algorithms, which have been recently used for the automatic detection of litter, mainly on beaches (Fallati et al., 2019; Gonçalves et al., 2020b), but also on the water surface (Jakovljevic et al., 2020; Kylili et al., 2019) (Table 2).

Studies to automatically detect marine litter in aerial imagery of beaches were conducted by Fallati et al. (2019) and Gonçalves et al. (2020b), who used a DJI Phantom 4 drone equipped with an RGB high resolution camera for the purpose, and developed a deep learning software for the automatic detection of litter. While the former authors reported a similar accuracy (0.95) to that obtained in the current study (0.85) for the training set, their F1-score for the testing set was lower (Table 2), probably due to the high detection of false negatives and false positives due to footprints and shadows on the beaches. Gonçalves et al. (2020b) also reported a lower F1-score than that obtained in the current study (Table 2), mainly due to the detection of many false positives. The main difficulties faced by the CNN model developed by these authors were related to the identification of litter items trapped among natural wood and dune vegetation.

Suitable algorithms that could deal with these environmental variables have still to be developed to improve the efficiency of new remote sensing technologies for routine beach monitoring. However, the challenges posed by the detection of floating litter over the marine surface are even more difficult to cope.

A deep learning algorithm to classify plastic litter in images from the water surface was recently developed by Jakovljevic et al. (2020), who used a DJI Mavic pro equipped with an RGB camera to take images of the surface of enclosed bodies of water with ground sampling distances similar to those used in the current study (0.4–3.0 cm vs 0.6–3.6 cm pixel^{-1}, respectively). The authors also deployed "positive controls" (plastic bottles, ropes, and

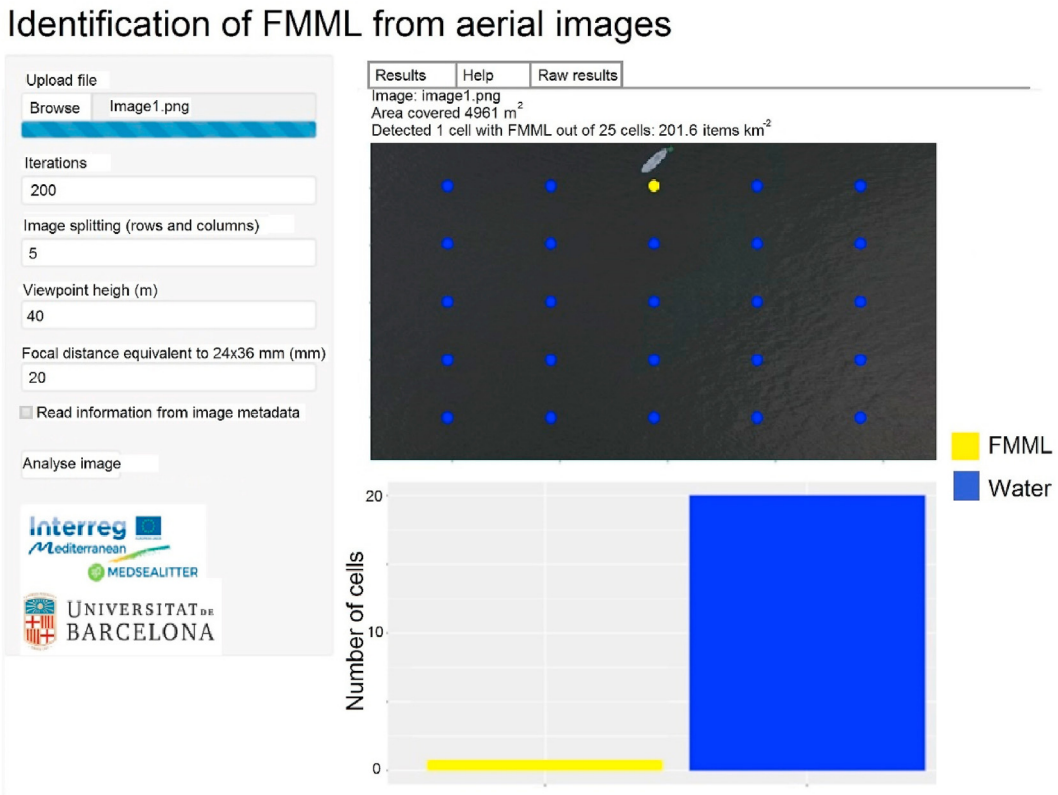

Fig. 7. Web-oriented application, named MARLIT, developed to detect interactively FMML in aerial images, based on the Shiny package. The MARLIT application can be downloaded from https://github.com/amonleong/MARLIT. On the left side of the app the user is able to: (1) browse and upload images, and specify: (2) the number of iterations used for the analysis, (3) the number of rows and columns for the image splitting, (4) the viewpoint height, and (5) the focal distance. Parameters for (2) and (3) should be at least 150 and 5 (to split the image into 25 cells), respectively. Information for (4) and (5) can be extracted directly from the image metadata. On the right side of the app, the panel shows the output of the analysis, including the image name, the area covered by the image, and the density of FMML detected. The above panel shows the image with its cells classified as containing FMML (yellow dots) and not containing FMML (blue dots); the bottom panel shows a histogram summarizing the number of cells containing and not containing FMML. (For interpretation of the references to color in this figure legend, the reader is referred to the Web version of this article.)

polystyrene) on the water surface to train their model, reporting similar F1-scores to those obtained in the current study (Table 2), and subsequently tested the CNN algorithm in an independent scenario, obtaining F1-scores for plastic and "maybe plastic" of 0.78 and 0.43, respectively. The low F1-score for "maybe plastic" was due to the confusion of this category with those of "water" and "plastic". However, although the methodology of Jakovljevic et al. (2020) is very similar to that applied here, their study was located in enclosed bodies of water (lakes), and thus some adverse elements (waves, foam, white caps) that may impair the detection of litter in the marine environment did not affect the performance of their algorithm.

Studies about automatic FMML detection in aerial RGB imagery are scarce: to the best of our knowledge, only Kylili et al. (2019) developed a CNN model for the automatic detection of FMML. The training and testing accuracies of the algorithms developed by these authors were higher than those obtained in the current study (Table 2). However, the images they used to test and train the model were taken from only a few meters above the sea surface, as their aim was the implementation of the model on a prototype device installed onboard marine vessels. Moreover, they used more images (9600) than those used here to train the CNN model, which may have been determinant to the higher level of accuracy attained (Sun et al., 2017).

The CNN algorithms presented in the current study were adapted from those currently available with the objective to streamline the process of FMML detection in images taken by aerial platforms (*e.g.*, drones, aircraft), which is highly time-demanding when performed by different trained scientists. As routine monitoring of FMML density, distribution, and trends is strongly recommended by national and international regulations, any improvement that would increase its efficiency and guarantee the consistency of results is highly valuable. Moreover, the development of user-friendly web-oriented applications such as MARLIT, the proof of concept presented here, may be of great interest for their implementation during regular monitoring of Marine Protected Areas, coastal areas, or even large oceanic areas. The current functionality of the application allows the user to upload aerial images and to get results in terms of presence and density of FMML and, if geo-referenced images are used, it could already provide an approximation of the presence of floating litter in a given marine area. The implementation of the CNN models developed in this study through a web-oriented application is a further step towards the automation of FMML detection and provides a useful approach to standardize FMML monitoring through any aerial platform (*e.g.*, a drone, or a small aircraft) equipped with remote sensing devices. It could be useful to classify high amounts of images as containing FMML or not, which in turn could help to identify potential areas of aggregation of litter at sea.

However, future improvements of the algorithm and the MARLIT application are needed to allow identifying the size, colour and type of FMML, which are relevant information for planning well-targeted policy and mitigation measures (GESAMP, 2019). The collaboration with other researchers to share data sets of sea

surface aerial imagery would also facilitate the improvement of the current model accuracy. As well, further research is needed to allow implementing the application directly to remote sensing devices for the real-time inspection of the marine surface during aerial surveys.

5. Conclusions

In this paper, we propose the use of CNN-based deep learning models connected to a web-oriented application to process aerial images for the automatic detection and quantification of FMML. Its installation in remote sensing devices, such as RGB cameras mounted on aerial platforms, would allow streamlining the monitoring of FMML over marine areas at any geographical scale. Further research is needed to improve the current automated algorithms by increasing the number of images used for training (and thus improving detection accuracy), and to implement the application directly on remote sensing devices. Effective and feasible automated methods to monitor FMML could complement or replace the traditional methods for marine monitoring, significantly improving the quality of results.

Declaration of competing interest

The authors declare that they have no known competing financial interests or personal relationships that could have appeared to influence the work reported in this paper.

Acknowledgements

Authors are grateful to the *EDMAKTUB* association, which provided the sailing catamaran and the infrastructure to perform some of the drone surveys; and to Eduardo Degollada, Bertrand Bouchard and *HEMAV* who provided the drones and the piloting expertise for making them fly. The authors are also grateful to the company 'Grup Airmed', which provided the Partenavia P-68 aircraft, the pilot and the infrastructure to perform the experiment, and the company *Geoxphere*, which provided the photographic camera and the support to operate it. Our sincere thanks to Professor Petia Radeva from the Faculty of Mathematics and Computer Science of the University of Barcelona, for her advice on the validation of the deep learning model during the final review. This study was supported by the project MEDSEALITTER (1 MED15_3.2_M12_334; European Union - European Regional Development Fund- Interreg MED). OGG's work was funded through a Ph.D. FPU scholarship granted by the Spanish Government. Constructive feedback from five anonymous reviewers substantially improved the manuscript.

Appendix A. Supplementary data

Supplementary data to this article can be found online at https://doi.org/10.1016/j.envpol.2021.116490.

Credit author statement

Odei Garcia-Garin: Conceptualization, Formal analysis, Investigation, Writing – original draft, Writing – review & editing, Visualization **Toni Monleón-Getino**: Methodology, Validation, Writing – review & editing, Supervision **Pere López-Brosa**: Methodology, Validation, Writing – review & editing **Asunción Borrell**: Resources, Supervision, Project administration, Funding acquisition **Alex Aguilar**: Resources, Supervision, Project administration, Funding acquisition **Ricardo Borja-Robalino**: Methodology, Validation, Writing – review & editing **Luis Cardona**: Resources, Funding acquisition **Morgana Vighi**: Conceptualization, Methodology, Resources, Writing – review & editing, Supervision

References

Arcangeli, A., Campana, I., Angeletti, D., Atzori, F., Azzolin, M., Carosso, L., et al., 2018. Amount, composition, and spatial distribution of floating macro litter along fixed trans-border transects in the Mediterranean basin. Mar. Pollut. Bull. 129 (2), 545–554. https://doi.org/10.1016/j.marpolbul.2017.02.026.

Bekkar, M., Kheliouane Djemaa, H., Akrouf Alitouche, T., 2013. Evaluation measure for models assessment over imbalanced data sets. J. Inf. Eng. Appl. 3, 27–38.

Bishop, C.M., 2006. Pattern Recognition and Machine Learning. Springer.

Chang, W., Cheng, J., Allaire, J., Xie, Y., McPherson, J., 2020. Shiny: web application framework for R. https://CRAN.R-project.org/package=shiny. R package version 1.4.0.2.

Chen, T., Kou, Q., He, T., 2018. MXNet: a flexible and efficient machine learning library for heterogeneous distributed systems. https://github.com/apache/incubator-mxnet/tree/master/R-package. R package version 1.2.0.

Cózar, A., Echevarría, F., González-Gordillo, J.I., Irigoien, X., Ubeda, B., Hernández-León, S., et al., 2014. Plastic debris in the open ocean. Proc. Natl. Acad. Sci. U.S.A. 111 (28), 10239–10244. https://doi.org/10.1073/pnas.1314705111.

De Stephanis, R., Giménez, J., Carpinelli, E., Gutierrez-Exposito, C., Cañadas, A., 2013. As main meal for sperm whales: plastics debris. Mar. Pollut. Bull. 69, 206–214. https://doi.org/10.1016/j.marpolbul.2013.01.033.

Deudero, S., Alomar, C., 2015. Mediterranean marine biodiversity under threat: reviewing influence of marine litter on species. Mar. Pollut. Bull. 98, 58–68. https://doi.org/10.1016/j.marpolbul.2015.07.012.

Dierssen, H.M., Garaba, S.P., 2020. Bright oceans: spectral differentiation of whitecaps, sea ice, plastics, and other flotsam. In: Vlahos, P., Monahan, E.C. (Eds.), Recent Advances in the Study of Oceanic Whitecaps: Twixt Wind and Waves. Springer International Publishing, Cham, pp. 197–208. https://doi.org/10.1007/978-3-030-36371-0_13.

Digka, N., Tsangaris, C., Torre, M., Anastasopoulou, A., Zeri, C., 2018. Microplastics in mussels and fish from the northern ionian sea. Mar. Pollut. Bull. 135, 30–40. https://doi.org/10.1016/j.marpolbul.2018.06.063.

Domènech, F., Aznar, F.J., Raga, J.A., Tomás, J., 2019. Two decades of monitoring in marine debris ingestion in loggerhead sea turtle, Caretta caretta, from the western Mediterranean. Environ. Pollut. 244, 367–378. https://doi.org/10.1016/j.envpol.2018.10.047.

Dumoulin, V., Visin, F., 2018. A guide to convolution arithmetic for deep learning. arXiv:1603.07285 [cs, stat]. http://arxiv.org/abs/1603.07285.

Falbel, D., Allaire, J.J., Chollet, F., RStudio, Google, Tang, Y., Van Der Bijl, W., Studer, M., Keydana, S., 2018. Keras, a high-level neural networks 'API'. https://CRAN.R-project.org/package=keras.%20R%20package%20version%202.2.5.0.

Fallati, L., Polidori, A., Salvatore, C., Saponari, L., Savini, A., Galli, P., 2019. Anthropogenic Marine Debris assessment with Unmanned Aerial Vehicle imagery and deep learning: a case study along the beaches of the Republic of Maldives. Sci. Total Environ. 693, 133581. https://doi.org/10.1016/j.scitotenv.2019.133581.

Fawcett, T., 2006. An introduction to ROC analysis. Pattern Recogn. Lett. 27 (8), 861–874. https://doi.org/10.1016/j.patrec.2005.10.010.

Galgani, F., Hanke, G., Werner, S., De Vrees, L., 2013. Marine litter within the European marine strategy framework directive. ICES (Int. Counc. Explor. Sea) J. Mar. Sci. 70 (6), 1055–1064. https://doi.org/10.1093/icesjms/fst176.

Garaba, S.P., Dierssen, H.M., 2018. An airborne remote sensing case study of synthetic hydrocarbon detection using short wave infrared absorption features identified from marine-harvested macro- and microplastics. Rem. Sens. Environ. 205, 224–235. https://doi.org/10.1016/j.rse.2017.11.023.

Garaba, S.P., Aitken, J., Slat, B., Dierssen, H.M., Lebreton, L., Zielinski, O., Reisser, J., 2018. Sensing ocean plastics with an airborne hyperspectral shortwave infrared imager. Environ. Sci. Technol. 52, 11699–11707. https://doi.org/10.1021/acs.est.8b02855 research-article.

Garcia-Garin, O., Vighi, M., Aguilar, A., Tsangaris, C., Digka, N., Kaberi, H., Borrell, A., 2019. *Boops boops* as a bioindicator of microplastic pollution along the Spanish Catalan coast. Mar. Pollut. Bull. 149 https://doi.org/10.1016/j.marpolbul.2019.110648.

Garcia-Garin, O., Aguilar, A., Borrell, A., Gozalbes, P., Lobo, A., Penadés-Suay, J., et al., 2020a. Who's better at spotting? A comparison between aerial photography and observer-based methods to monitor floating marine litter and marine mega-fauna. Environ. Pollut. 258 https://doi.org/10.1016/j.envpol.2019.113680.

Garcia-Garin, O., Borrell, A., Aguilar, A., Cardona, L., Vighi, M., 2020b. Floating marine macro-litter in the north western Mediterranean Sea: results from a combined monitoring approach. Mar. Pollut. Bull. 159, 111467. https://doi.org/10.1016/j.marpolbul.2020.111467.

Garcia-Garin, O., Sala, B., Aguilar, A., Vighi, M., Víkingsson, G.A., Chosson, V., et al., 2020c. Organophosphate contaminants in North Atlantic fin whales. Sci. Total Environ. 721, 137768. https://doi.org/10.1016/j.scitotenv.2020.137768.

Garcia-Garin, O., Vighi, M., Sala, B., Aguilar, A., Tsangaris, C., Digka, N., et al., 2020d. Assessment of organophosphate flame retardants in Mediterranean *Boops boops* and their relationship to anthropization levels and microplastic ingestion. Chemosphere 252, 126569. https://doi.org/10.1016/j.chemosphere.2020.126569.

GESAMP, 2015. Sources, fate and effects of microplastics in the marine environment: a global assessment. In: Kershaw, P.J. (Ed.), IMO/FAO/UNESCO- IOC/

UNIDO/WMO/IAEA/UN/UNEP/UNDP Joint Group of Experts on the Scientific Aspects of Marine Environmental Protection. Rep. Stud. GESAMP No. 90, 96. International Maritime Organization, London, UK.
GESAMP, 2019. Guidelines for the monitoring and assessment of plastic litter in the ocean. GESAMP Rep. Stud. 99, 130.
Goddijn-Murphy, L., Dufaur, J., 2018. Proof of concept for a model of light reflectance of plastics floating on natural waters. Mar. Pollut. Bull. 135, 1145–1157. https://doi.org/10.1016/j.marpolbul.2018.08.044.
Goddijn-Murphy, L., Peters, S., van Sebille, E., James, N.A., Gibb, S., 2018. Concept for a hyperspectral remote sensing algorithm for floating marine macro plastics. Mar. Pollut. Bull. 126, 255–262. https://doi.org/10.1016/j.marpolbul.2017.11.011.
Gonçalves, G., Andriolo, U., Pinto, L., Bessa, F., 2020a. Mapping marine litter using UAS on a beach-dune system: a multidisciplinary approach. Sci. Total Environ. 706, 135742. https://doi.org/10.1016/j.scitotenv.2019.135742.
Gonçalves, G., Andriolo, U., Pinto, L., Duarte, D., 2020b. Mapping marine litter with Unmanned Aerial Systems : a showcase comparison among manual image screening and machine learning techniques. Mar. Pollut. Bull. 155, 111158. https://doi.org/10.1016/j.marpolbul.2020.111158.
Guirado, E., Tabik, S., Rivas, M.L., Alcaraz-Segura, D., Herrera, F., 2019. Whale counting in satellite and aerial images with deep learning. Sci. Rep. 9, 1–12. https://doi.org/10.1038/s41598-019-50795-9.
Jakovljevic, G., Govedarica, M., Alvarez-Taboada, F., 2020. A deep learning model for automatic plastic mapping using unmanned aerial vehicle (UAV) data. Rem. Sens. 12, 1515. https://doi:10.3390/rs12091515.
Kako, S., Morita, S., Taneda, T., 2020. Estimation of plastic marine debris volumes on beaches using unmanned aerial vehicles and image processing based on deep learning. Mar. Pollut. Bull. 155, 111127. https://doi.org/10.1016/j.marpolbul.2020.111127.
Kikaki, A., Karantzalos, K., Power, C.A., Raitsos, D.E., 2020. Remotely sensing the source and transport of marine plastic debris in bay islands of Honduras (caribbean sea). Rem. Sens. 12, 1727. https://doi.org/10.3390/rs12111727.
Kuo, C.C.J., 2016. Understanding convolutional neural networks with a mathematical model. J. Vis. Commun. Image Represent. 41, 406–413. https://doi.org/10.1016/j.jvcir.2016.11.003.
Kylili, K., Kyriakides, I., Artusi, A., Hadjistassou, C., 2019. Identifying floating plastic marine debris using a deep learning approach. Environ. Sci. Pollut. Control Ser. 26 (17), 17091–17099. https://doi.org/10.1007/s11356-019-05148-4.
Lebreton, L., Slat, B., Ferrari, F., Sainte-Rose, B., Aitken, J., Marthouse, R., et al., 2018. Evidence that the great pacific garbage Patch is rapidly accumulating plastic. Sci. Rep. 8 (1), 1–15. https://doi.org/10.1038/s41598-018-22939-w.
Martin, C., Parkes, S., Zhang, Q., Zhang, X., McCabe, M.F., Duarte, C.M., 2018. Use of unmanned aerial vehicles for efficient beach litter monitoring. Mar. Pollut. Bull. 131, 662–673. https://doi.org/10.1016/j.marpolbul.2018.04.045.
Martínez-Vicente, V., Clark, J.R., Corradi, P., Aliani, S., Arias, M., Bochow, M., et al., 2019. Measuring marine plastic debris from space: initial assessment of observation requirements. Rem. Sens. 11 (20), 8–14. https://doi.org/10.3390/rs11202443.
Matthews, J.P., Ostrovsky, L., Yoshikawa, Y., Komori, S., Tamura, H., 2017. Dynamics and early post-tsunami evolution of floating marine debris near Fukushima Daiichi. Nat. Geosci. 10, 598–603. https://doi.org/10.1038/NGEO2975.
Maximenko, N., Corradi, P., Law, K.L., Sebille, E. Van, Garaba, S.P., Lampitt, R.S., et al., 2019. Towards the integrated marine debris observing system. Frontiers in Marine Science 6. https://doi.org/10.3389/fmars.2019.00447.
Merlino, S., Paterni, M., Berton, A., Massetti, L., 2020. Unmanned aerial vehicles for debris survey in coastal areas: long-term monitoring programme to study spatial and temporal accumulation of the dynamics of beached marine litter. Rem. Sens. 12 (8), 1–23. https://doi.org/10.3390/RS12081260.
Pichel, W.G., Veenstra, T.S., Churnside, J.H., Arabini, E., Friedman, K.S., Foley, D.G., et al., 2012. GhostNet marine debris survey in the Gulf of Alaska - satellite guidance and aircraft observations. Mar. Pollut. Bull. 65, 28–41. https://doi.org/10.1016/j.marpolbul.2011.10.009.
Quetglas, A., Ordines, F., Guijarro, B., 2011. The use of artificial neural networks (ANNs) in aquatic ecology. Artificial neural networks - application. https://doi.org/10.5772/16092.
R Core Team, 2020. R: A Language and Environment for Statistical Computing. R Foundation for Statistical Computing, Vienna, Austria. https://www.R-project.org/.
Schuyler, Q., Hardesty, B.D., Wilcox, C., Townsend, K., 2014. Global analysis of anthropogenic debris ingestion by sea turtles. Conserv. Biol. 28, 129–139. https://doi: 10.1111/cobi.12126.
Shridhar, K., Laumann, F., Liwicki, M., 2019. A comprehensive guide to bayesian convolutional neural network with variational inference. CoRR, 1–38. Retrieved from. http://arxiv.org/abs/1901.02731.
Suaria, G., Aliani, S., 2014. Floating debris in the Mediterranean Sea. Mar. Pollut. Bull. 86, 494–504. https://doi.org/10.1016/j.marpolbul.2014.06.025.
Suaria, G., Perold, V., Lee, J.R., Lebouard, F., Aliani, S., Ryan, P.G., 2020. Floating macro- and microplastics around the southern ocean: results from the antarctic circumnavigation expedition. Environ. Int. 136, 105494. https://doi.org/10.1016/j.envint.2020.105494.
Sun, C., Shrivastava, A., Singh, S., Gupta, A., 2017. Revisiting unreasonable effectiveness of data in deep learning era. IEEE International Conference on Computer Vision (ICCV) 843–852.
Topouzelis, K., Papakonstantinou, A., Garaba, S.P., 2019. Detection of floating plastics from satellite and unmanned aerial systems (Plastic Litter Project 2018). Int. J. Appl. Earth Obs. Geoinf. 79, 175–183. https://doi.org/10.1016/j.jag.2019.03.011.
UNEP, 2005. UNEP. In: Marine Litter: an Analytical Overview.
UNEP, 2016. Marine Plastic Debris and Microplastics – Global Lessons and Research to Inspire Action and Guide Policy Change. United Nations Environment Programme, Nairobi.
Van Sebille, E., Aliani, S., Law, K.L., Maximenko, N., Alsina, J.M., Bagaev, A., et al., 2020. The physical oceanography of the transport of floating marine debris. Environ. Res. Lett. 15, 023003 https://doi.org/10.1088/1748-9326/ab6d7d.
Veenstra, T.S., Churnside, J.H., 2012. Airborne sensors for detecting large marine debris at sea. Mar. Pollut. Bull. 65, 63–68. https://doi.org/10.1016/j.marpolbul.2010.11.018.
Velandia, N.S., Hernandez Beleno, R.D., Jimenez Moreno, R., 2017. Applications of deep neural networks. Int. J. Syst. Signal Contr. Eng. Appl. 10 (1–6), 61–76.